Effect of TiO2 nanoparticle loading on Poly(l-lactic acid) porous scaffolds fabricated by TIPS

Effect of TiO_2 nanoparticle loading on Poly(L-lactic acid) porous scaffolds fabricated by TIPS

Aleksandra Buzarovska [a, *], Chiara Gualandi [b], Annapaola Parrilli [c], Mariastella Scandola

[a] Faculty of Technology and Metallurgy, RudjerBoskovic 16, 1000, Skopje, Macedonia
[b] Department of Chemistry "G.Ciamician"University of Bologna, Via Selmi2, 40126, Bologna, Italy
[c] Biocompatibility, Technological Innovations and Advanced Therapies Laboratory - BITTA, Rizzoli Orthopedic Institute, Via di Barbiano 1/10, 40136, Bologna, Italy

A B S T R A C T

Porous nanocomposite scaffolds of poly(L-lactic acid) (PLA), loaded with TiO_2 nanoparticles, were prepared by thermally induced phase-separation (TIPS). The preparation procedure induced crystalline polymer structures (with degree of crystallinity up to 51%) with no evidence of residual solvent, as confirmed by thermal analysis. Scaffold porosity, distribution of the nanofiller and shape of the pores were investigated by X-ray micro computed tomography (μ-CT) and scanning electron microscopy (SEM). The produced scaffolds with porosity of 86 ± 2% have interconnected open tubular pores with diameter and length in the ranges 40–80 μm and 200–400 μm respectively. The inorganic TiO_2 nano-additive is well dispersed in the scaffold walls, with only a small fraction of micrometric aggregates observable. All investigated polymer scaffolds display similar compressive moduli (between 2.1 and 2.8 MPa). Thermogravimetry (TGA), wide angle X-ray diffraction (XRD) and SEM analyses run on scaffolds subjected to *in vitro* mineralization tests showed that PLA scaffolds loaded with TiO_2 develop an amount of hydroxyapatite four times higher than that of plain PLA, thus assessing that titania nanoparticles confer improved bioactivity to the scaffolds.

1. Introduction

In the last 20 years biodegradable and bioactive porous scaffolds consisting of polymer/inorganic composites have been intensively investigated for application in bone tissue engineering [1–4]. Composite systems combining advantages of polymers and of inorganic substances offer a promising approach to overcome the drawbacks encountered when single-component scaffolds are used [5]. Polymers can be easily processed with a number of scaffold fabrication techniques to obtain controllable and reproducible porous architectures and they have tunable degradation rate, however they are poorly bioactive and are thus scarcely useful for inducing bone regeneration [1]. Therefore, bioactive inorganic substances have been introduced in polymer matrices in order to confer bioactivity to the scaffolds. Inorganic materials with composition close to the mineral phase of bone, such as bioglasses and calcium phosphates, are highly osteoconductive and capable to integrate well into the host bone [6]. Moreover, their use in combination with a polymer phase enables to counteract their intrinsic brittleness and low resistance to break propagation.

There is still some ambiguity surrounding the optimal porosity and pore size for a 3D bone scaffold. Typically, a porosity of 80–90% and a minimum pore size of 50–100 μm have been quoted for achieving cell penetration, proper vascularization and bone formation [7–9]. Several review articles describe the desired properties of scaffolds for bone tissue engineering and their fabrication technologies [10–12]. Commonly used processes for the production of such scaffolds are phase separation, foaming and solvent casting/particulate leaching. Thermally induced phase separation (TIPS) has been largely applied in the production of scaffolds for bone tissue engineering. This technique enables to produce highly porous structures (up to 95%) with highly interconnected micrometric pores. Pore dimension, morphology and orientation can be controlled by varying polymer concentration in solution, solvent and cooling temperature [13].

In this work polymer/inorganic composite scaffolds of Poly(L-lactic acid) (PLA) loaded with titanium oxide nanoparticles were produced by TIPS. PLA is a degradable polymer largely employed in

* Corresponding author. Tel.: +389 2 3088 207.
E-mail address: abuzar@tmf.ukim.edu.mk (A. Buzarovska).

Please cite this article in press as: Buzarovska A, et al., Effect of TiO_2 nanoparticle loading on Poly(L-lactic acid) porous scaffolds fabricated by TIPS, Composites Part B (2015), http://dx.doi.org/10.1016/j.compositesb.2015.07.016

the biomedical field for medium to long-term implants. TiO_2 has been employed as filler of polymer matrices for different biomedical applications, including scaffolds for bone tissue engineering [14–16], drug delivery [16–19] and devices with antibacterial properties [16]. In addition, TiO_2 nanoparticles were proven to be more effective than microparticles in improving osteoblast functions (adhesion, synthesis of alkaline phosphatase, and deposition of calcium-containing mineral) [20]. Earlier work reported that the Ti–OH surface groups of the crystalline forms of titanium oxide, especially those of anatase, are capable to induce epitaxial nucleation of hydroxyapatite from simulated body fluid (SBF) [21,22].

Although it was mentioned that TiO_2 nanoparticles impart bioactivity on PLA, the aim of this study is to perform a careful investigation of 3D architecture of PLA and TiO_2-loaded scaffolds and to evaluate their applicability for bone tissue engineering. Since μ-CT technique enables to detect and visualize 3D nanoparticle agglomerates as well as their dimensions, the main focus of this paper is to highlight the volumetric distribution of TiO_2 filler within the polymer matrix and to correlate it with the thermal, structural and bioactivity characteristics of the prepared scaffolds.

2. Experimental part

2.1. Materials and methods

Poly(L-lactic acid) (PLA) used in this study (M_w = 220 kDa, M_n = 101 kDa) was purchased from Biomer (Krailling, Germany). Titanium oxide (TiO_2) nanopowder (Hombicat UV100, average particle size = 5 nm, BET surface area > 250 m^2/g, 99% anatase) was a product of Sachtleben Chemie GmbH. The solvents (dioxane and ethanol) were Merck products and were used without additional purification.

2.2. Preparation of PLA/TiO_2 nanocomposite scaffolds

The PLA/TiO_2 nanocomposite scaffolds were prepared using thermally induced phase separation (TIPS). Two alternative methods of solvent removal were applied: freeze-extraction or freeze-drying. PLA was dissolved in dioxane at 50 °C and stirred for two days in a glass vial. A given amount of nanopowder was suspended in dioxane and ultrasonicated for 30 min. The polymer solution and TiO_2-dioxane suspension were mixed to produce a 5% (w/v) PLA-dioxane solution. The resulting mixture was ultrasonicated for additional 30 min and then frozen at −30 °C in a deep freezer.

Freeze-extraction procedure After 24 h, the frozen mixture was removed from the glass vial and soaked in a beaker filled with precooled ethanol at −30 °C. The frozen sample was maintained in a freezer at 4 °C for three days, while the solvent was changed every 24 h. After complete dioxane extraction, the sample was vacuum dried at room temperature. Sample labels and compositions are listed Table 1.

Table 1
Polymer scaffolds prepared by TIPS.

Sample	Solvent removal method	PLA/TiO_2 w/w (%)
PLA	freeze-extraction	100/0
PLA/TiO_2-5	freeze-extraction	95/5
PLA/TiO_2-10	freeze-extraction	90/10
d-PLA	freeze-drying	100/0
d-PLA/TiO_2-5	freeze-drying	95/5
d-PLA/TiO_2-10	freeze-drying	90/10

Freeze-drying procedure The frozen mixture was freeze-dried at −20 °C and 10^{-3} mbars for 72 h. Sample labels and compositions are listed Table 1.

2.3. Scaffold mineralization

In vitro mineralization tests were performed using a slightly supersaturated CaP solution, which was prepared as previously reported [23]. In brief, a Ca solution (5 mM $CaCl_2 \cdot 2H_2O$) and a P solution (36 mM $NaHCO_3$ and 5 mM $Na_2HPO_4 \cdot 12H_2O$) were prepared in double distilled water and buffered at pH = 7.2 with Hepes [4-(2-hydroxyethyl)-1-piperazineethanesulfonic acid]. CaP supersaturated calcifying solution was freshly prepared before performing the experiments, by mixing equal volumes of Ca and P solutions at 37 °C. Mineralization experiments were run on PLA and PLA/TiO_2-10 scaffolds. The scaffolds were soaked in the supersaturated solution at 37 °C and were kept at this temperature for 6 h under mild shaking. After completing the treatment, scaffolds were carefully washed with distilled water and vacuum dried overnight.

2.4. Scaffold characterization

Thermogravimetric analyses (TGA) were performed under nitrogen flow at a heating rate of 10 °C min^{-1}, from room temperature to 500 °C, using a TA Instruments TGA2950.

Differential Scanning Calorimetry (DSC) measurements were performed using a TA Instruments DSC-2910. The samples were heated from −20 °C up to 220 °C at a heating rate of 20 °C/min. The degree of crystallinity (χ_c) was determined by applying the following equation:

$$\frac{\Delta H_m}{\Delta H_m^0 \cdot w_{PLA}} \cdot 100 \quad (1)$$

where ΔH_m is the experimental melting enthalpy, ΔH_m^0 the melting enthalpy of 100% crystalline PLA taken as 93.2 J/g [24] and w_{PLA} is PLA weight fraction.

X-ray diffraction analysis (XRD) was performed using X-ray Diffractometer, (PANalyticalX'Pert PRO equipped with an X'Celerator detector), with CuK_α radiation (λ = 0.154 nm). The measurements were performed in the 2θ range between 5 and 60°, collecting for 80 s at each scan step of 0.065°.

The morphology of the inner part of the scaffolds was observed with a Philips 515 scanning electron microscope (SEM) at an accelerating voltage of 15 kV. Prior to SEM analysis, samples were sputter-coated with gold.

Full assessment of the porous structure, porosity, pore size and distribution of the nano filler was performed with microcomputed tomography (μ-CT, Skyscan 1172, Bruker Micro-CT, Kontich, Belgium) with applied voltage of 20 kV and a current of 110 μA. During the scan, the samples were rotated by 180° with a step of 0.3°. The obtained jpg images (μ-CT cross-sections) had 4000×4000 pixels each with a pixel size of 2 μm. Microstructural characteristics were determined using CTAn software, while the orientation of pores was evaluated using OrientationJ, an ImageJ plug-in Ref. [25].

Compressive mechanical properties were determined at room temperature, using a TA.XT Stable Micro System, UK. Cylindrical samples with diameter of 20 mm and 5 mm height were analyzed using static load of 5 kg and cross-head speed of 1 mm min^{-1}. The compressive moduli were calculated from the initial linear region of stress–strain curves. Five replicate specimens were run for each sample and results are provided as the average value ± standard deviation.

Please cite this article in press as: Buzarovska A, et al., Effect of TiO_2 nanoparticle loading on Poly(L-lactic acid) porous scaffolds fabricated by TIPS, Composites Part B (2015), http://dx.doi.org/10.1016/j.compositesb.2015.07.016

3. Results and discussion

3.1. Thermal and structural characterization of the scaffolds

Thermogravimetric analysis was performed to gain information about thermal degradation of the polymer, possible presence of residual solvent and actual amount of TiO_2 in the scaffold. TGA curves of the scaffolds are reported in Fig. 1 while Table 2 lists the corresponding relevant parameters. All thermogravimetric curves display a main weight loss in the temperature range 300–400 °C, corresponding to the thermal degradation of PLA, and a residual weight at 500 °C that is reasonably close to the nominal content of TiO_2 in the scaffolds (5 or 10 wt%). The weight loss observed at T < 120 °C in the samples prepared by freeze-drying can be ascribed to residual solvent, demonstrating that this scaffold preparation procedure does not allow the complete evaporation of solvent, as previously found when freeze-drying was applied to prepare poly(lactide-co-glycolide) scaffolds [26]. The same authors showed that the residual solvent can be eliminated by washing the freeze-dried scaffolds in ethanol, a step that, however, lengthens the scaffold preparation procedure [26]. Conversely, in Fig. 1 no weight loss ascribable to residual solvent is detected in TGA curves of the samples prepared by the freeze-extraction method. Hence freeze-extracted scaffolds were selected and the following characterization results refer to them. In order to quantify the amount of crystallinity developed by PLA during scaffold preparation, DSC first scans of the samples (not shown) were analyzed. No cold crystallization peak was observed during the heating scan and all samples exhibited a single melting endotherm with T_m = 171 °C. This result shows that crystallization of PLA (both primary and secondary crystallization) was completed during scaffold fabrication. The degree of crystallinity (χ_c, Table 2), calculated from the DSC curves by means of Equation (1), slightly increases with increasing content of TiO_2 nanoparticles in the scaffold, possibly due to an earlier reported nucleating effect of titania on PLA crystallization [27–29].

Table 2
Thermal characterization of scaffolds.

Sample	Δm (%)[a]	Residue (%)[b]	X_c (%)[c]
PLA	0.05	2.0	46.4
PLA/TiO_2-5	0.002	6.4	48.9
PLA/TiO_2-10	0.04	10.5	51.0
d-PLA	1.7	2.2	n.d.[d]
d-PLA/TiO_2-5	2.6	6.1	n.d.
d-PLA/TiO_2-10	1.9	10.9	n.d.

[a] From RT to 120 °C.
[b] At 500 °C.
[c] By DSC, normalized with respect to the actual PLA content in the given scaffold.
[d] Not determined.

XRD patterns of PLA and of its nanocomposite scaffolds, with distinctive crystalline peaks, are given in Fig. 2. It can be observed that XRD pattern for pure PLA scaffold shows an intensive reflection at 2θ = 16.6° and a less intense peak at 2θ = 19.0°, corresponding respectively to the (110/200) and (203/113) planes of the orthorombic lattice of the α-form [30]. The XRD profile of the nanocomposite scaffold filled with 10 wt% of TiO_2 shows additional peaks at 25.3°, 37.9°, 48.0°and 54.4° (broad), that are attributed to (101), (004), (200) and (105 and 211) planes of the TiO_2 anatase phase respectively [31]. The introduction of the nanofiller does not affect the evolved crystalline structure of PLA that is in all samples α-form.

3.2. Morphological characterization of the scaffolds

The freeze-extracted cylindrical scaffolds produced by TIPS (Fig. 3A) were analyzed by μ-CT to gain information about total porosity, size and shape of the pores, and TiO_2 distribution. All scaffolds are characterized by high open porosity (86 ± 2%) whereas

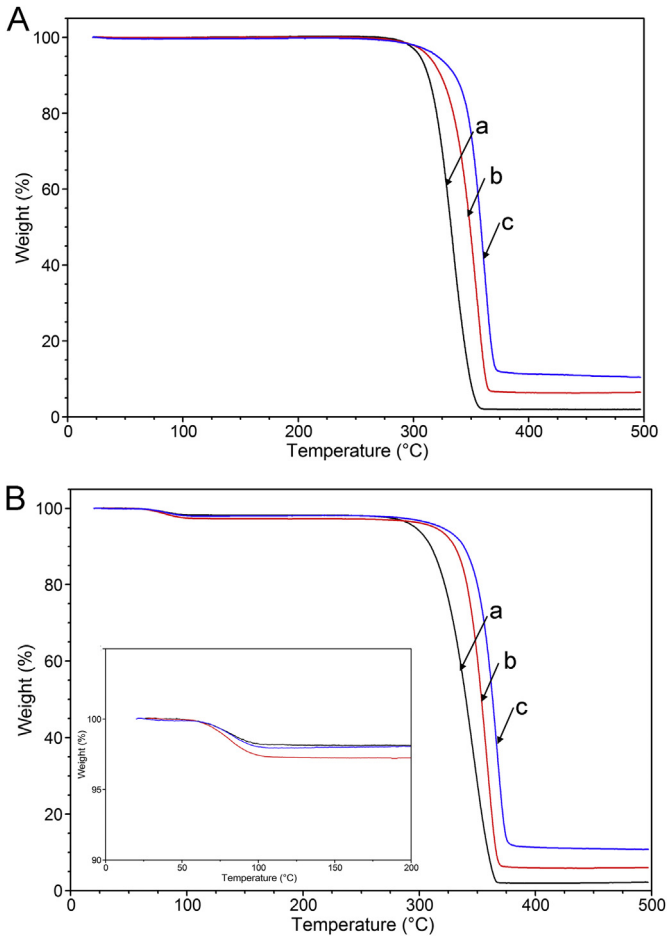

Fig. 1. TGA curves of PLA (a), PLA/TiO_2-5 (b) and PLA/TiO_2-10 (c) scaffolds, produced by freeze extraction (A) or freeze drying (B).

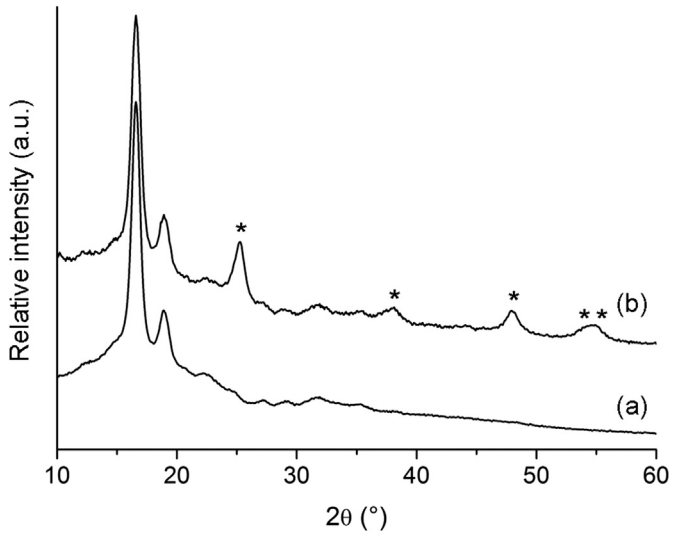

Fig. 2. X-ray diffraction patterns of PLA (a) and PLA/TiO_2-10 (b). The asterisks highlight the anatase peaks.

Please cite this article in press as: Buzarovska A, et al., Effect of TiO_2 nanoparticle loading on Poly(L-lactic acid) porous scaffolds fabricated by TIPS, Composites Part B (2015), http://dx.doi.org/10.1016/j.compositesb.2015.07.016

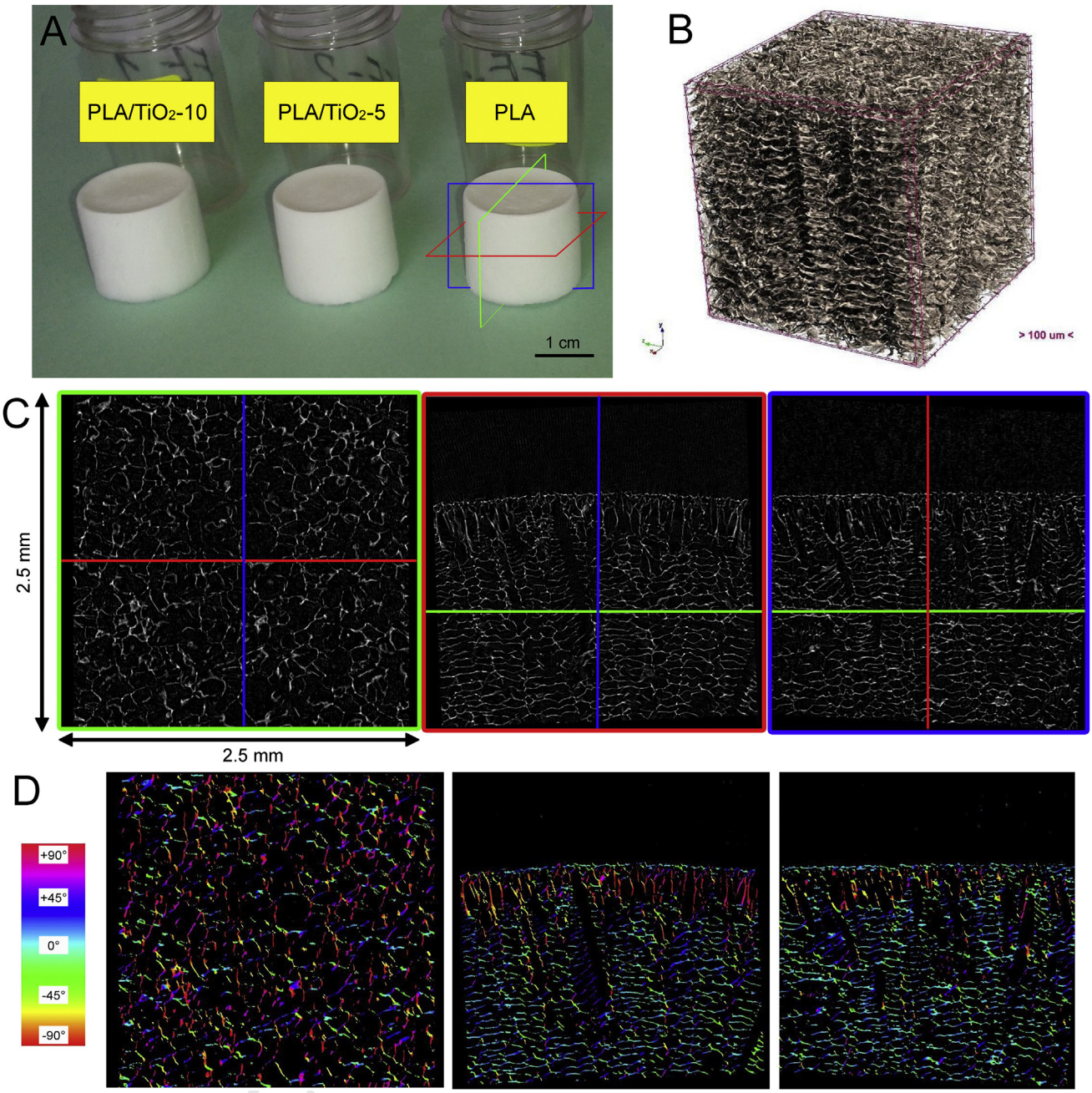

Fig. 3. Picture of the freeze extracted scaffolds produced by TIPS (A) and μ-CT results on PLA scaffold (B, C, D). (B) 3-Dμ-CT model of a scaffold portion.(C) two-dimensional μ-CT cross-sections: colored squares around each μ-CT picture identify the section space orientation, shown as colored Cartesian planes in A. (D) two-dimensional μ-CT cross-sections where scaffold walls are colored according to their angular orientation with respect to the tangent to scaffold edge.

no closed porosity is detected, demonstrating complete interconnection of scaffold pores. The latter is a key feature to enable scaffold vascularization, cell colonization, tissue ingrowth and nutrient exchange in *in vivo* applications. Fig. 3B shows a three-dimensional (3-D) μ-CT reconstruction of a representative portion of the PLA scaffold, whereas 2-D images of scaffold cross-sections are reported in Fig. 3C. Inspection of the scaffold cross-sections highlights the presence of tubular pores, most of them having diameter and length in the ranges 40–80 μm and 200–400 μm, respectively. Close to the scaffold edge the channels tend to be perpendicular to the scaffold surface down to a depth of about 300 μm. This particular pore orientation (highlighted in Fig. 3D using a graded colored scale) is attributed to the presence of a radial temperature gradient in the outer scaffold shell during scaffold fabrication by TIPS. Such a T gradient generates when the vial containing the polymer solution is stored in the freezer and it influences the process of pore formation via solvent separation/solidification. Indeed, it was previously demonstrated that strongly anisotropic pore structures are generated by well-defined temperature gradients during TIPS scaffold fabrication, as a consequence of solvent crystals growing along the gradient direction [32–34]. The effect associated with the T-gradient in the present scaffolds seems to vanish at a distance from the surface of ca. 300 μm where channel orientation tends to become parallel to the outer scaffold surface (Fig. 3D).

The pore architecture illustrated in Fig. 3 for PLA was also found in the μ-CT analysis of the scaffolds loaded with TiO_2. The SEM images of Fig. 4 confirm such a morphology. When scaffold walls

Please cite this article in press as: Buzarovska A, et al., Effect of TiO_2 nanoparticle loading on Poly(L-lactic acid) porous scaffolds fabricated by TIPS, Composites Part B (2015), http://dx.doi.org/10.1016/j.compositesb.2015.07.016

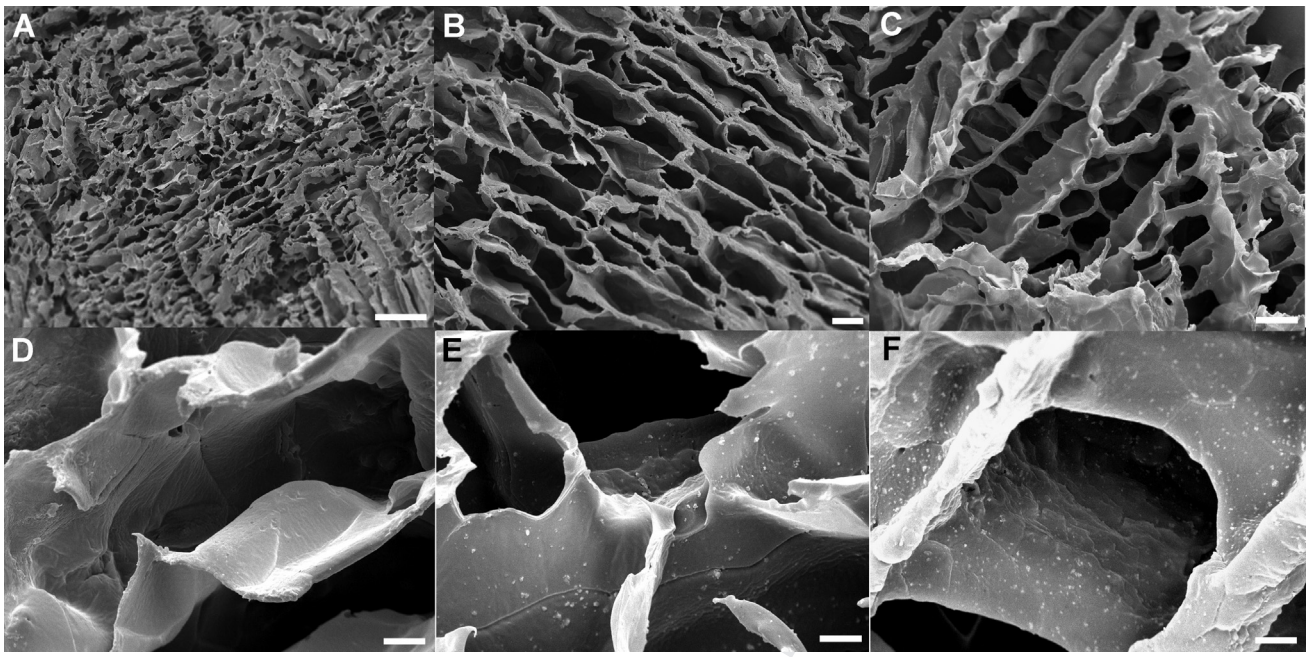

Fig. 4. SEM images of the morphology of scaffolds obtained by freeze extraction (A, B and C: pictures refer to PLA scaffold and are also representative of TiO_2-loaded scaffolds). Magnifications refer to PLA (D), PLA/TiO_2-5 (E) and PLA/TiO_2-10 (F) scaffolds. Scale bars: A = 200 μm; B and C = 50 μm; D, E and F = 10 μm.

are observed at high magnification (Fig. 4D, E and F) the boundaries of large spherulitic structures seem to appear, in agreement with the DSC evidence of highly crystalline scaffolds. SEM images of samples loaded with TiO_2 display small white dots on scaffold walls (Fig. 4E and F) with diameter ranging from few nanometers (visible at higher magnification) to few micrometers. The μ-CT technique enables to detect and visualize 3-D TiO_2 agglomerates with dimension greater than or equal to nearly 2 μm in the loaded scaffolds. Fig. 5 shows the 3-D μ-CT reconstruction of a representative portion of PLA/TiO_2-10 and highlights the corresponding volumetric distribution of TiO_2 particles (colored in blue). The titania agglomerates, whose average dimension in terms of diameter of the equivalent-volume sphere is in the range of a few microns (Fig. 5C), are seen to be homogeneously distributed in the PLA/TiO_2-10 scaffold (Fig. 5B). Their amount, calculated from μ-CT, is about 0.88% by volume that corresponds to 2.6% by weight. Therefore we can conclude that, although the nano-dispersion of TiO_2 is not optimal, micrometric agglomerates are few and about 75% by weight of the loaded titania is finely dispersed in particles with sub-micrometric dimensions. This result can be probably ascribed to the fact that, when the TiO_2 suspension is frozen, formation of large agglomerates is impaired in the viscous polymeric dioxane solution.

The mechanical properties of the 3D scaffolds are generally governed by their porosity. The compressive moduli were determined from the linear part of the stress–strain curves and very similar values were obtained for all scaffolds (E_{PLA} = 2.8 ± 0.6 MPa, $E_{PLA/TiO_{2-5}}$ = 2.9 ± 0.9 MPa, $E_{PLA/TiO_{2-10}}$ = 2.2 ± 0.3 MPa). This behavior may be associated to the fact that the porosity of all investigated scaffolds (86 ± 2) did not change with TiO_2 loadings.

The literature reports for PLA scaffolds with high porosity (above 80%) modulus values in the range 1–10 MPa, depending on the material and on scaffold density [32,33,35,36]. Numerous studies have also shown minimal increase of the mechanical properties or even decrease with increasing content of the filler [37,38]. The present compressive modulus data confirm that the

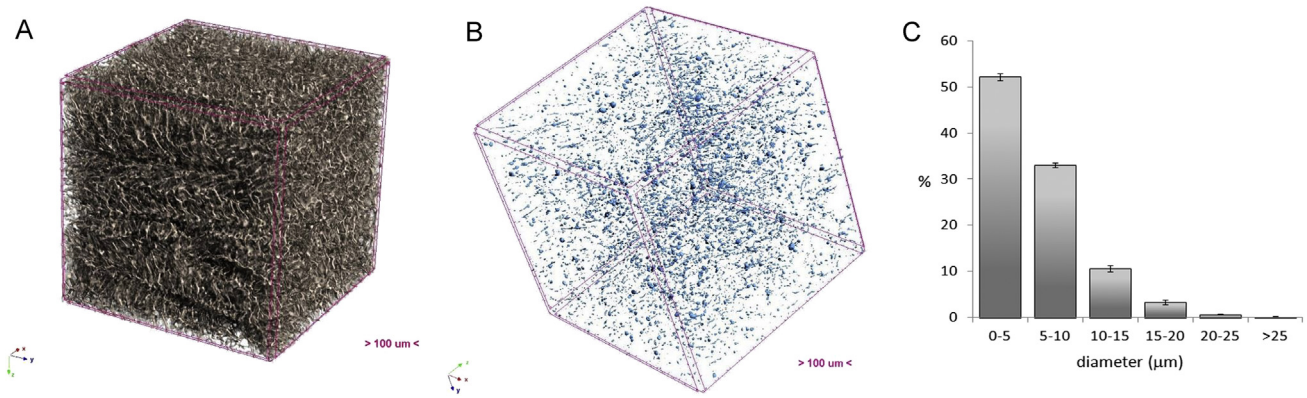

Fig. 5. PLA/TiO_2-10 scaffold:3-D μ-CT model of a portion of the scaffold (A), the corresponding volumetric distribution of TiO_2 agglomerates detected by μ-CT (≥2 μm, in blue) (B) and TiO_2particle size distribution in terms of volume-equivalent sphere diameters (C). (For interpretation of the references to colour in this figure legend, the reader is referred to the web version of this article.)

Please cite this article in press as: Buzarovska A, et al., Effect of TiO_2 nanoparticle loading on Poly(L-lactic acid) porous scaffolds fabricated by TIPS, Composites Part B (2015), http://dx.doi.org/10.1016/j.compositesb.2015.07.016

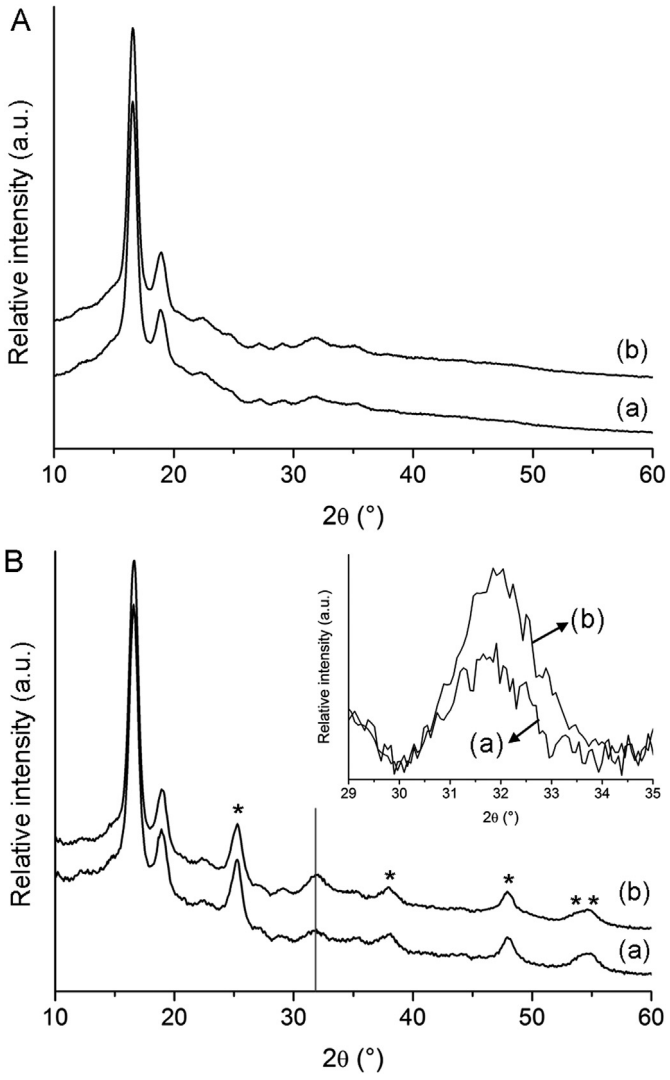

Fig. 6. XRD patterns of PLA (A) and PLA/TiO_2-10 (B) scaffolds before (a) and after 6 h of immersion in Ca/P solution (b). The vertical line is in the position where hydroxyapatite shows the most intense peaks. The asterisks highlight the anatase peaks. In B an enlarged view of the range 29–35° is reported in the inset.

mechanical properties of the scaffolds are not significantly influenced by TiO_2 in the concentration range investigated, even when the filler is well distributed as demonstrated by μ-CT and SEM results.

3.3. Scaffold mineralization

In this work mineralization experiments were carried out by using a slightly supersaturated Ca/P solution that induces a very fast deposition of hydroxyapatite on both inorganic and polymeric substrates [23,39] and is characterized by an ionic composition simpler than that of SBF. In order to evaluate the effect of the presence of TiO_2 on scaffold mineralization, PLA and PLA/TiO_2-10 samples were immersed in the supersaturated Ca/P solution for 6 h. The samples retrieved from the solution were analyzed by TGA, XRD and SEM. TGA analysis showed for both scaffolds an increase of the solid residue at 500 °C after 6 h in contact with Ca/P solution. Such an increment, associated with the mineralization process, was larger for PLA/TiO_2-10 (4%) than for PLA (1%).

The XRD patterns of pristine scaffolds and of mineralized scaffolds are shown in Fig. 6. The formation of hydroxyapatite is expected to show main reflections at $2\theta = 26°$ and around $2\theta = 32°$, the latter being due to three intense peaks that are overlapped in poor crystalline material [40]. It is worth pointing out that the mentioned reflections fall where reflections of TiO_2 and of PLA are observed in the scaffolds before mineralization. In Fig. 6A the XRD pattern of PLA mineralized sample is similar to that of the pristine scaffold, in line with the very low increment of inorganic content in this sample after mineralization (1wt% by TGA). Conversely, the pattern of mineralized PLA/TiO_2-10 (Fig. 6B) shows a clear intensity increase around $2\theta = 32°$, whereas no significant enhancement of the diffractogram intensity appears at $2\theta = 26°$, where the typical anatase peak also lays. The observed increment of the pattern intensity at $2\theta = 32°$, where hydroxyapatite shows the most intense peaks, is a clear evidence of its presence in this sample. The SEM micrographs of PLA and PLA/TiO_2-10 mineralized scaffolds are shown in Fig. 7. It is seen that the walls of both scaffolds are coated with a mineralized layer. On PLA the inorganic phase seems to cover the scaffold surface rather homogeneously with particles having diameter in the range 100–400 nm. Conversely, at the surface of the PLA/TiO_2-10 scaffold, individual microparticles with the typical 'cauliflower' morphology of hydroxyapatite crystals [23,41] are observed. The inhomogeneous distribution of such

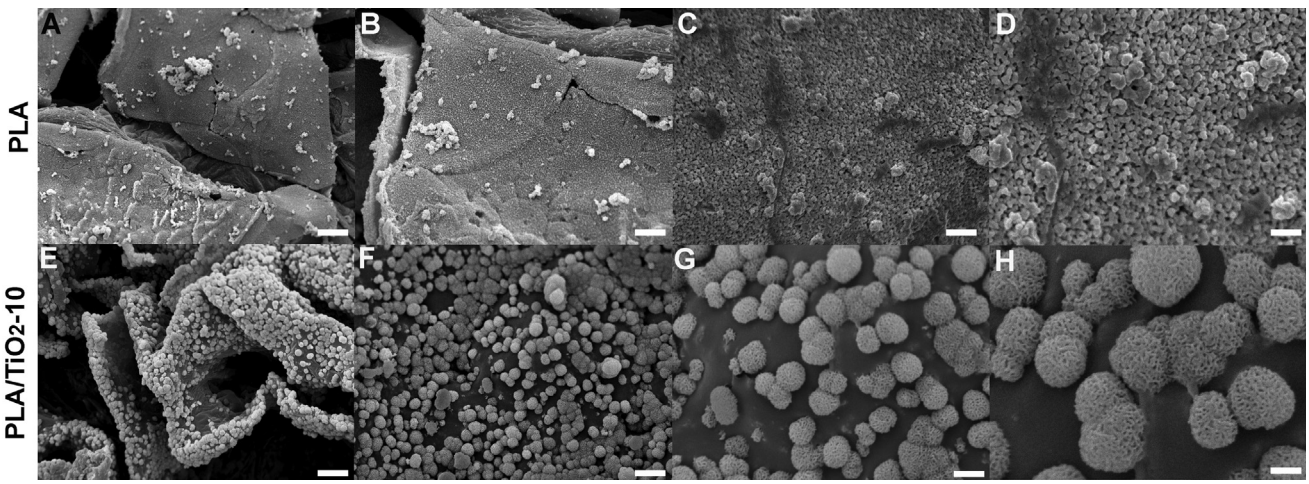

Fig. 7. SEM images of PLA scaffold (A–D) and PLA/TiO_2-10 scaffold (E–H) after 6 h of immersion in Ca/P solution at different magnifications. Scale bars: A, E = 10 μm; B, F = 5 μm; C, G = 2 μm; D, H = 1 μm.

Please cite this article in press as: Buzarovska A, et al., Effect of TiO_2 nanoparticle loading on Poly(L-lactic acid) porous scaffolds fabricated by TIPS, Composites Part B (2015), http://dx.doi.org/10.1016/j.compositesb.2015.07.016

crystal clusters on the surface of the scaffold pores may be attributed in PLA/TiO_2-10 to the presence of titania particles. Indeed the ability of crystalline titanium oxide, particularly in the anatase form, to induce crystallization of hydroxyapatite [22,23,41] likely via epitaxial crystallization [21] is well documented. The absence of 'cauliflower' agglomerates on plain PLA (Fig. 7, A–D) is attributed to slower HA crystallization in such a scaffold that lacks the nucleating TiO_2 inorganic component. It is expected that the 'cauliflower' morphology might appear also in plain PLA at longer mineralization times, as already found in other unloaded polymeric scaffolds [39].

4. Conclusions

PLLA/TiO_2 nanocomposite scaffolds with two different contents of titania (5 and 10 wt. %) were obtained via thermally induced phase-separation, where dioxane was used as a solvent for PLLA matrix. Highly crystalline structures were produced, with no significant effect of the nanofiller on their evolvement. Careful investigation of the scaffolds by μ-CT and SEM analyses highlighted their suitability for bone tissue engineering application: scaffolds display high porosity (86 ± 2%), with open and interconnected pores, having diameter and length in the ranges 40–80 μm and 200–400 μm, respectively, ideal for achieving cell penetration and proper vascularization. μ-CT analysis enabled to localize the inorganic TiO_2 nano-additive in the scaffold walls and showed its good dispersion, with only a small fraction of micrometer aggregates observable. The effect of TiO_2 nanoparticles on scaffold mineralization was clearly demonstrated. Indeed, after 6 h in Ca/P supersaturated solution the loaded scaffold contained an amount of hydroxyapatite, with the typical 'cauliflower' morphology, four times higher than that of the plain PLA scaffold.

Acknowledgments

This work was partially supported by a JoinEU-SEE>PENTA grant to A.B. The authors would like to acknowledge Dr. Massimo Gazzano for his help in interpretation of XRD data.

References

[1] Masami O, Baiju J. Synthetic biopolymer nanocomposites for tissue engineering scaffolds. Prog Polym Sci 2013;38:1487–503.
[2] Li J, Baker AB, Mou X, Ren N, Qiu J, Boughton IR, et al. Biopolymer/calcium phosphate scaffolds for bone tissue engineering. Adv Healthc Mater 2014;3:469–84.
[3] Johnson AJW, Herschler BA. A review of the mechanical behavior of CaP and CaP/polymer composites for applications in bone replacement and repair. Acta Biomater 2011;7:16–30.
[4] Rezwan K, Chen QZ, Blaker JJ, Boccaccini AR. Biodegradable and bioactive porous polymer/inorganic composite scaffolds for bone tissue engineering. Biomaterials 2006;27:3413–31.
[5] Guarino V, Gloria A, Raucci MG, De Santis R, Ambrosio L. Bio-inspired composite and cell instructive platforms for bone regeneration. Int Mater Rev 2012;57:256–75.
[6] Best SM, Porter AE, Thian ES, Huang J. Bioceramics: past, present and for the future. J Eur Ceram Soc 2008;28:1319–27.
[7] Klawitter JJ, Bagwell JG, Weinstein AM, Sauer BW, Pruitt JR. An evaluation of bone growth into porous high density polyethylene. J Biomed Mater Res 1976;10:311–23.
[8] Lu JX, Flautre B, Anselme K, Hardouin P, Gallur A, Descamps M, et al. Role of interconnections in porous bioceramics on bone recolonization in vitro and in vivo. J Mater Sci Mater M 1999;10:111–20.
[9] Hing KA. Bioceramic bone graft substitutes: influence of porosity and chemistry. Int J Appl Ceram Technol 2005;2:184–99.
[10] Hutmacher DW. Scaffolds in tissue engineering bone and cartilage. Biomaterials 2000;21:2529–43.
[11] Salgado AJ, Coutinho OP, Reis RL. Bone tissue engineering: state of the art and future trends. Macromol Biosci 2004;4:743–65.
[12] Amini AR, Laurencin CT, Nukavarapu SP. Bone tissue engineering: recent advances and challenges. Crit Rev Biomed Eng 2012;40:363–408.
[13] Akbarzadeh R, Yousefi AM. Effects of processing parameters in thermally induced phase separation technique on porous architecture of scaffolds for bone tissue engineering. J Biomed Mater Res B 2014;102:1304–15.
[14] Divyarani VV, Ramachandran R, Chennazhi KP, Tamura H, Nair SV, Jayakumar R. Fabrication of alginate/nanoTiO_2 needle composite scaffolds for tissue engineering applications. Carbohydr Polym 2011;83:858–64.
[15] Jayakumar R, Ramachandran R, Divyarani VV, Chennazhi KP, Tamura H, Nair SV. Fabrication of chitin–chitosan/nano TiO_2-composite scaffolds for tissue engineering applications. Int J Biol Macromol 2011;48:336–44.
[16] Wu S, Weng Z, Liu X, Yeung KWK, Chu PK. Functionalized TiO_2 based nanomaterials for biomedical applications. Adv Funct Mater 2014;24:5464–81.
[17] Chen C, Lv G, Pan C, Song M, Wu C, Guo D, et al. Poly(lactic acid) (PLA) based nanocomposites—a novel way of drug-releasing. Biomed Mater 2007;2:L1–4.
[18] Signoretto M, Ghedini E, Nichele V, Pinna F, Crocellà V, Cerrato G. Effect of textural properties on the drug delivery behaviour of nanoporous TiO_2 matrices. Microporous Mesoporous Mater 2011;139:189–96.
[19] Jiang H, Wang T, Wang L, Sun C, Jiang T, Cheng G, et al. Development of an amorphous mesoporous TiO_2 nanosphere as a novel carrier for poorly water-soluble drugs: effect of different crystal forms of TiO_2 carriers on drug loading and release behaviors. Microporous Mesoporous Mater 2012;153:124–30.
[20] Webster TJ, Smith TA. Increased osteoblast function on PLGA composites containing nanophase titania. J Biomed Mater Res A 2005;74:677–86.
[21] Uchida M, Kim HM, Kokubo T, Fujibayashi S, Nakamura T. Structural dependence of apatite formation on titania gels in a simulated body fluid. J Biomed Mater Res A 2003;64:164–70.
[22] Kokubo T, Kim KM, Kawashita M. Novel bioactive materials with different mechanical properties. Biomaterials 2003;24:2161–75.
[23] Bigi A, Boanini E, Bracci B, Facchini A, Panzavolta S, Segatti F, et al. Nanocrystalline hydroxyapatite coatings on titanium: a new fast biomimetic method. Biomaterials 2005;26:4085–9.
[24] Barndup J, Immergut EH. Polymer handbook. New York (: Wiley Interscience; 1988.
[25] Rezakhaniha R, Agianniotis A, Schrauwen JT, Griffa A, Sage D, Bouten CV, et al. Experimental investigation of collagen waviness and orientation in the arterial adventitia using confocal laser scanning microscopy. Biomech Model Mechanobiol 2012;11:461–73.
[26] Cao Y, Crol ITI, O'Connor AJ, Stevens GW, Cooper-White JJ. Systematic selection of solvents for fabrication of 3D combined macro- and microporous polymeric scaffolds for soft tissue engineering. J Biomater Sci Polym E 2006;17:369–402.
[27] Buzarovska A, Grozdanov A. Biodegradable Poly(L-lactic acid)/TiO_2 nanocomposites.: thermal properties and degradation. J Appl Polym Sci 2012;123:2187–93.
[28] Luo YB, Li WD, Wang XL, Xu DY, Wang YZ. Preparation and properties of nanocomposites based on poly(lactic acid) and functionalized TiO_2. Acta Mater 2009;57:3182–91.
[29] Liao R, Yang B, Yu W, Zhou C. Isothermal cold crystallization kinetics of polylactide/nucleating agents. J Appl Polym Sci 2007;104:310–7.
[30] De Santis P, Kovacs AJ. Molecular conformation of poly(S-lactic acid). Biopolymers 1968;6:299–306.
[31] Powder Diffraction File n. 21–1272, International Centre for Diffraction Data (ICDD), Newtown Square, PA (USA).
[32] Ma PX, Zhang R. Microtubular architecture of biodegradable polymer scaffolds. J Biomed Mater Res 2001;56:469–77.
[33] Yang F, Qu X, Cui W, Bei J, Yu F, Lu S, et al. Manufacturing and morphology structure of polylactide-type microtubules orientation- structured scaffolds. Biomaterials 2006;27:4923–33.
[34] Hu X, Shen H, Yang F, Bei J, Wang S. Preparation and cell affinity of microtubular orientation-structured PLGA(70/30) blood vessel scaffold. Biomaterials 2008;29:3128–36.
[35] Wei G, Ma PX. Structure and properties of nano-hydroxyapatite/polymer composite scaffolds for bone tissue engineering. Biomaterials 2004;25:4749–57.
[36] Boccaccini AR, Blaker JJ, Maquet V, Chung W, Jeome R, Nazhat SN. Poly(D,L-lactide) (PDLLA) foams with TiO_2 nanoparticles and PDLLA/TiO_2-bioglass® foam composites for tissue engineering scaffolds. J Mater Sci 2006;41:3999–4008.
[37] Cai X, Tong H, Shen X, Chen W, Yan J, Hu J. Preparation and characterization of homogeneous chitosan–polylactic acid/hydroxyapatite nanocomposite for bone tissue engineering and evaluation of its mechanical properties. Acta Biomater 2009;5:2693–703.
[38] Cui Y, Liu Y, Cui Y, Jing X, Zhang P, Chen X. The nanocomposite scaffold of poly(lactide-co-glycolide) and hydroxyapatite surface-grafted with L-lactic acid oligomer for bone repair. Acta Biomater 2009;5:2680–92.
[39] Torricelli P, Gioffrè M, Fiorani A, Panzavolta S, Gualandi C, Fini M, et al. Co-electrospun gelatin-poly(L-lactic acid) scaffolds: modulation of mechanical properties and chondrocyte response as a function of composition. Mater Sci Eng C 2014;36:130–8.
[40] Powder Diffraction File n. 9–432, International Centre for Diffraction Data (ICDD), Newtown Square, PA (USA).
[41] Wei J, Chen QZ, Stevens MM, Roether JA, Boccaccini AR. Biocompatibility and bioactivity of PDLLA/TiO_2 and PDLLA/TiO_2/Bioglass® nanocomposites. Mater Sci Eng C 2008;28:1–10.

Please cite this article in press as: Buzarovska A, et al., Effect of TiO_2 nanoparticle loading on Poly(L-lactic acid) porous scaffolds fabricated by TIPS, Composites Part B (2015), http://dx.doi.org/10.1016/j.compositesb.2015.07.016